Supplementary material

Insights into secondary organic aerosol formation from the day- and nighttime oxidation of PAHs and furans in an oxidation flow reactor

Abd El Rahman El Mais[1,2], Barbara D'Anna[2], Luka Drinovec[3], Andrew T. Lambe[4], Zhe Peng[5], Jean-Eudes Petit[6], Olivier Favez[1], Selim Aït-Aïssa[1], Alexandre Albinet[1]

[1]Ineris, Parc Technologique Alata, Verneuil-en-Halatte, 60550, France
[2]Aix Marseille Univ, CNRS, LCE, Marseille, France
[3]Center for Atmospheric Research, University of Nova Gorica, Nova Gorica, Slovenia
[4]Aerodyne Research, Inc. (ARI), Billerica, Massachusetts, USA
[5]CIRES and Department of Chemistry, University of Colorado, Boulder, Colorado 80309, USA
[6]Laboratoire des Sciences du Climat et de l'Environnement (LSCE), 91190 Gif sur Yvette, France

Correspondence to: Alexandre Albinet (alexandre.albinet@ineris.fr)

1

Table of Contents

45   **TABLES**

Table S1. Radical exposures in the PAM-OFR during both day and nighttime oxidation processes.

SOA precursor	OH exp (molecules cm^{-3} s)		NO$_3$ exp (molecules cm^{-3} s)
	Experimental evaluation	KinSim calculations	
2-MF	8.09×10^{11}	1.13×10^{12}	1.68×10^{12}
2,5-DMF	4.05×10^{11}	7.61×10^{11}	5.15×10^{12}
Furan	nd[1]	1.05×10^{10}	*
Naph	3.74×10^{11}	2.78×10^{11}	2.10×10^{14}
Acy	1.05×10^{12}	1.51×10^{12}	6.44×10^{13}
Flu	2.19×10^{12}	2.57×10^{12}	**
Phe	1.46×10^{12}	1.96×10^{12}	2.08×10^{14}

[1]not determined.

*Unstable furan injection inducing an unstable SOA generation.

**No SOA formed.

50   **Table S2. Photon fluxes at 185 nm (I_{185}) and 254 nm (I_{254}) used as inputs to the OFR KinSim model in the case of OH radical. They were obtained by varying the model input flux values while keeping an I_{185} to I_{254} ratio of 0.0664 (Rowe et al., 2020) until the model output O$_3$ concentrations matched with [O$_3$]$_{PAM}$.**

SOA precursor	[O$_3$]$_{PAM}$ (ppm)	I_{185} (photons cm^{-2} s^{-1})	I_{254} (photons cm^{-2} s^{-1})
2-MF	15	8.2×10^{13}	1.23×10^{15}
2,5-DMF	12	7.18×10^{13}	1.08×10^{15}
Furan	7	3.38×10^{13}	5.09×10^{14}
Naph	3	1.41×10^{13}	2.12×10^{14}
Acy	4	2.03×10^{13}	3.06×10^{14}
Flu	11	5.88×10^{13}	8.86×10^{14}
Phe	10	4.85×10^{13}	7.30×10^{14}

Table S3. Bimolecular rate coefficients of the studied SOA precursors with OH, NO$_3$, and O$_3$ and their UV photo-absorption cross sections at/near 185 and 254 nm.

SOA precursor	Bimolecular rate coefficients (cm^3 molecule^{-1} s^{-1})			Photo-absorption cross sections (σ_i) (cm^2 molecule^{-1})	
	k_{OH}	k_{NO_3}	k_{O_3}	λ = 185 nm	λ = 254 nm
2-MF	7.00 x 10^{-11} [a]	2.57 x 10^{-11} [b]	8.50 x 10^{-17} [c]	8.36 x 10^{-18} [Δj]	3.79 x 10^{-19} [Δj]
2,5-DMF	1.16 x 10^{-10} [a]	5.78 x 10^{-11} [b]	4.20 x 10^{-16} [d]	8.36 x 10^{-18} [*]	3.79 x 10^{-19} [*]
Furan	3.83 x 10^{-11} [a]	1.30 x 10^{-12} [d]	2.42 x 10^{-18} [d]	1.18 x 10^{-17} [Δk]	2.59 x 10^{-19} [Δk]
Naph	2.30 x 10^{-11} [a]	4.60 x 10^{-17} [e]	< 2.00 x 10^{-19} [e]	2.67 x 10^{-17} [Δl]	1.09 x 10^{-17} [Δm]
Acy	1.09 x 10^{-10} [a]	5.45 x 10^{-12} [f]	5.50 x 10^{-16} [f]	7.92 x 10^{-17} [n]	2.74 x 10^{-17} [n]
Flu	1.31 x 10^{-11} [a]	1.52 x 10^{-14} [g]	< 2.00 x 10^{-19} [h]	7.89 x 10^{-17} [n]	2.57 x 10^{-17} [n]
Phe	2.40 x 10^{-11} [a]	1.20 x 10^{-13} [i]	4.00 x 10^{-19} [i]	2.44 x 10^{-17} [Δl]	3.06 x 10^{-17} [Δl]

55   [a](Database for the Kinetics of the Gas-Phase Atmospheric Reactions of Organic Compounds). [b](Kind et al., 1996). [c](Li et al., 2018). [d](Jiang et al., 2020). [e](Keyte et al., 2013). [f](Atkinson and Aschmann, 1988). [g](Ding et al., 2020). [h](Kwok et al., 1997). [i](Kwok et al., 1994).

[Δ](The MPI-Mainz UV/VIS Spectral Atlas of Gaseous Molecules of Atmospheric Interest). [j](Giuliani et al., 2003). [k](Christianson et al., 2021). [l](Kitagawa, 1968). [m](Grosch et al., 2015). [n](Theoretical spectral database of PAHs).

60   [*]No information available in the literature. Assumed equal to the ones of 2-MF.

Table S4. Fixed filter loading compensation parameters k(λ) used to manually compensate the AE33 data for each SOA precursor with the studied oxidant given the large jumps observed during the spot changes.

SOA Precursor	Reactivity	Wavelength (nm)			
		370	**470**	**520**	**590**
		k (λ)			
Naph	OH	0.00350	0.00570	0.02129	0.03687
	NO$_3$	0.00496	0.00665	0.02961	0.06053
Acy	OH	0.00444	0.00578	0.00034	0.01140
	NO$_3$	0.00376	0.00054	0.02944	0.07180
Flu	OH	0.00234	0.00610	0.03821	0.08846
	NO$_3$	*	*	*	*
Phe	OH	0.00492	0.01600	0.05480	0.12789
	NO$_3$	**	**	**	**

* No data are shown for Flu with NO$_3$ radicals because no SOA were formed.

**No jumps observed during the spot changes so no manual compensation was done. The same was obtained with furan SOA under both OH and NO$_3$ reactivities.

Table S5. Air mass absorption efficiency values used for AE33 data (Drinovec et al., 2015).

Channel	1	2	3	4	5	6	7
Wavelength (nm)	370	470	520	590	660	880	950
σ_{air} (m^2 g^{-1})	18.47	14.54	13.14	11.58	10.35	7.77	7.19

Table S6. Slope, intercept, and regression of the linear fit of ln (b_{abs}) as a function of ln (λ) over the wavelength range 370 - 590 nm used to evaluate the absorption Ångström exponent (α).

	Slope	Intercept	R^2
OH radical			
Naph	-5.4329	-87.9898	0.9570
Acy	-8.3516	-132.1933	0.9939
Flu	-6.0803	-99.4019	0.9803
Phe	-6.9225	-112.1611	0.9951
NO$_3$ radical			
Naph	-5.5670	-89.6167	0.9665
Acy	-6.7757	-107.7455	0.9698
Flu	-	-	-
Phe	-7.0470	-115.1764	0.9910

70

Table S7. Comparison of Absorption Ångström exponent (α) and Mass Absorption cross section (MAC) obtained for naphthalene SOA with literature data.

| Experimental conditions	Methodology	λ range (nm)	α	MAC, 400-405 nm (m² g⁻¹)	References
OH, OFR, without NO$_x$, RH = 41%	7λ AE33	370 - 590	5.43 ± 0.15	0.22	This study
NO$_3$, OFR, without NO$_x$, RH = 43%			5.57 ± 0.12	0.22	
OH, smog chamber, low NO$_x$, RH = 0 - 89 %	UV-Vis measurements of SOA filter extracts	280 - 680	$5.5 - 7.6$	0.15-0.26	(Klodt et al., 2023)
OH, smog chamber, high NO$_x$, RH = 0 - 94 %				0.2-0.35	
OH, OFR, NO$_x$, RH = 39%	HPLC equipped with a photodiode array detector and electrospray ionization HR-MS	315 - 650	-	0.22-0.38	(He et al., 2022)
OH, OFR, low NO$_x$, RH = 38%	HPLC equipped with a photodiode array detector and electrospray ionization HR-MS	300 - 450	8.87	0.12	(Siemens et al., 2022)
OH, OFR, high NO$_x$, RH = 38%			7.59	0.19	
OH, smog chamber, H$_2$O$_2$, RH = 12 - 15%	UV-Vis measurements of SOA filter extracts	300 - 550	6.46 ± 0.25	0.35	(Xie et al., 2017)
OH, smog chamber, high NO$_x$, RH = 10 - 19%			4.92 ± 0.23	0.78	
OH, smog chamber, high NO$_x$, dry	UV-Vis measurements of SOA filter extracts	400 - 630	6.2	0.12	(Lee et al., 2014)
OH, OFR, without NO$_x$, RH = 30 - 40%	UV-Vis measurements of SOA filter extracts and cavity ring-down photoacoustic spectrometry	300 - 500	5.2 - 6.6	0.02 – 0.09	(Lambe et al., 2013)
OH, smog chamber, high NOx, seed, RH < 5%	3λ photoacoustic soot spectrometer (PASS-3)	405 - 781	>3.53	0.81 ± 0.32	(Metcalf et al., 2013)
OH, smog chamber, without NO$_x$, RH < 2%	UV-Vis measurements of SOA filter extracts	400 - 630	6.2	0.07	(Updyke et al., 2012)
OH, smog chamber, with NO$_x$, RH < 2%			6.7	0.22	

75
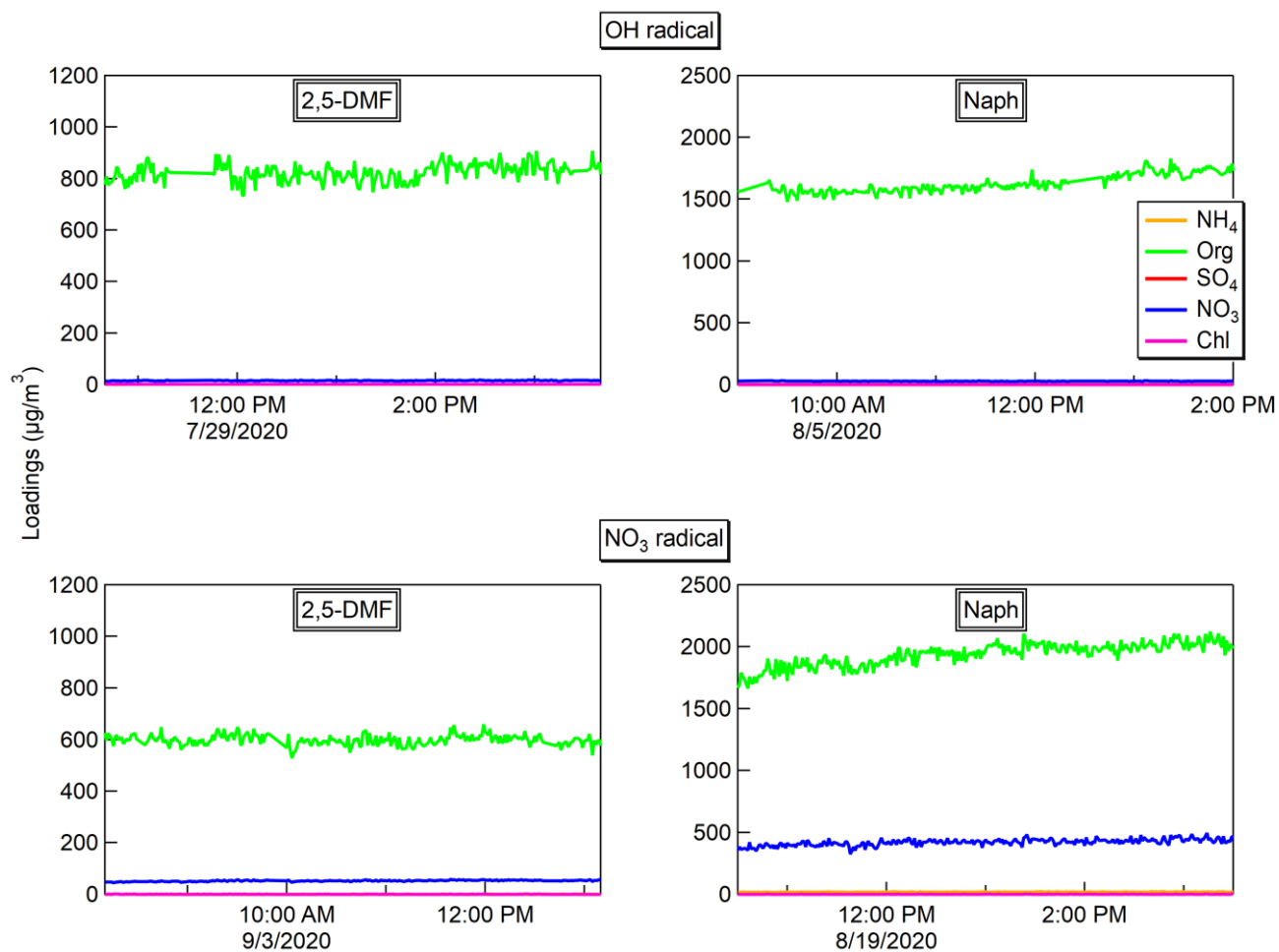
Figure S1. Examples of Q-ACSM measurements showing the stable PAHs and furans SOA generation through day- and nighttime oxidation processes during experiments lasting up to 5 hours.
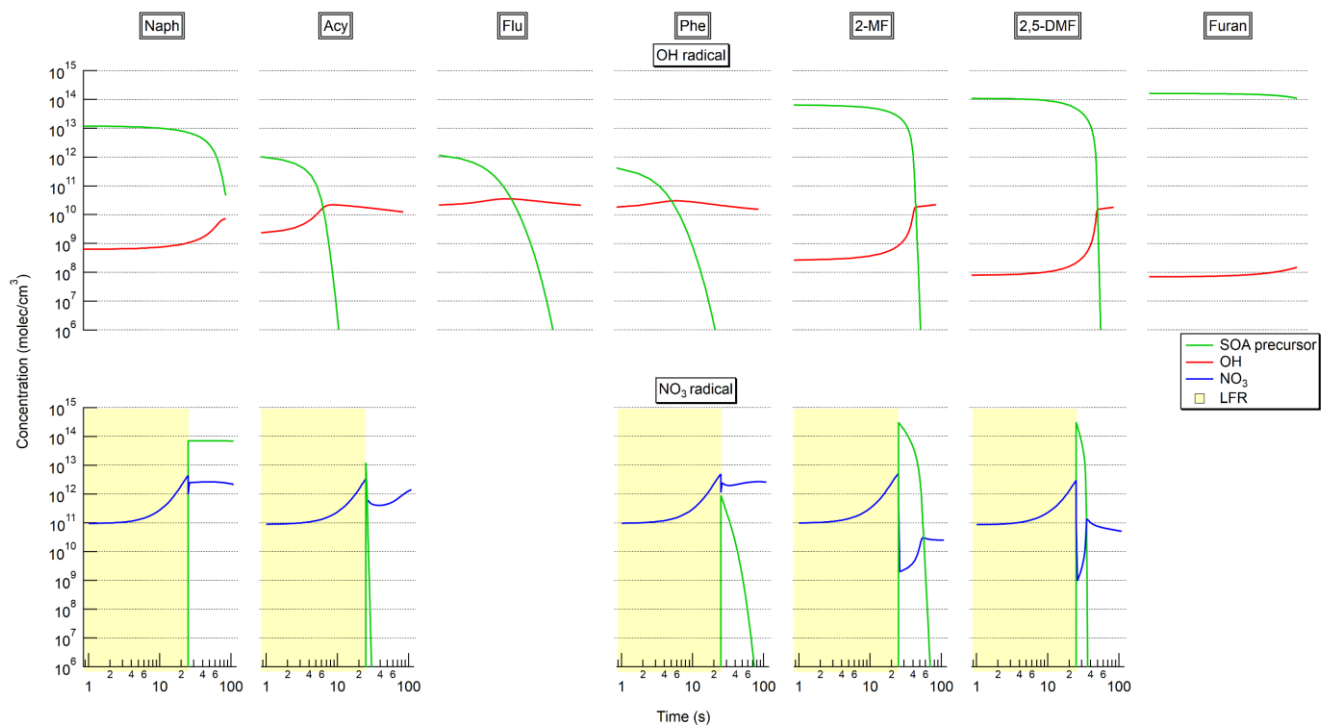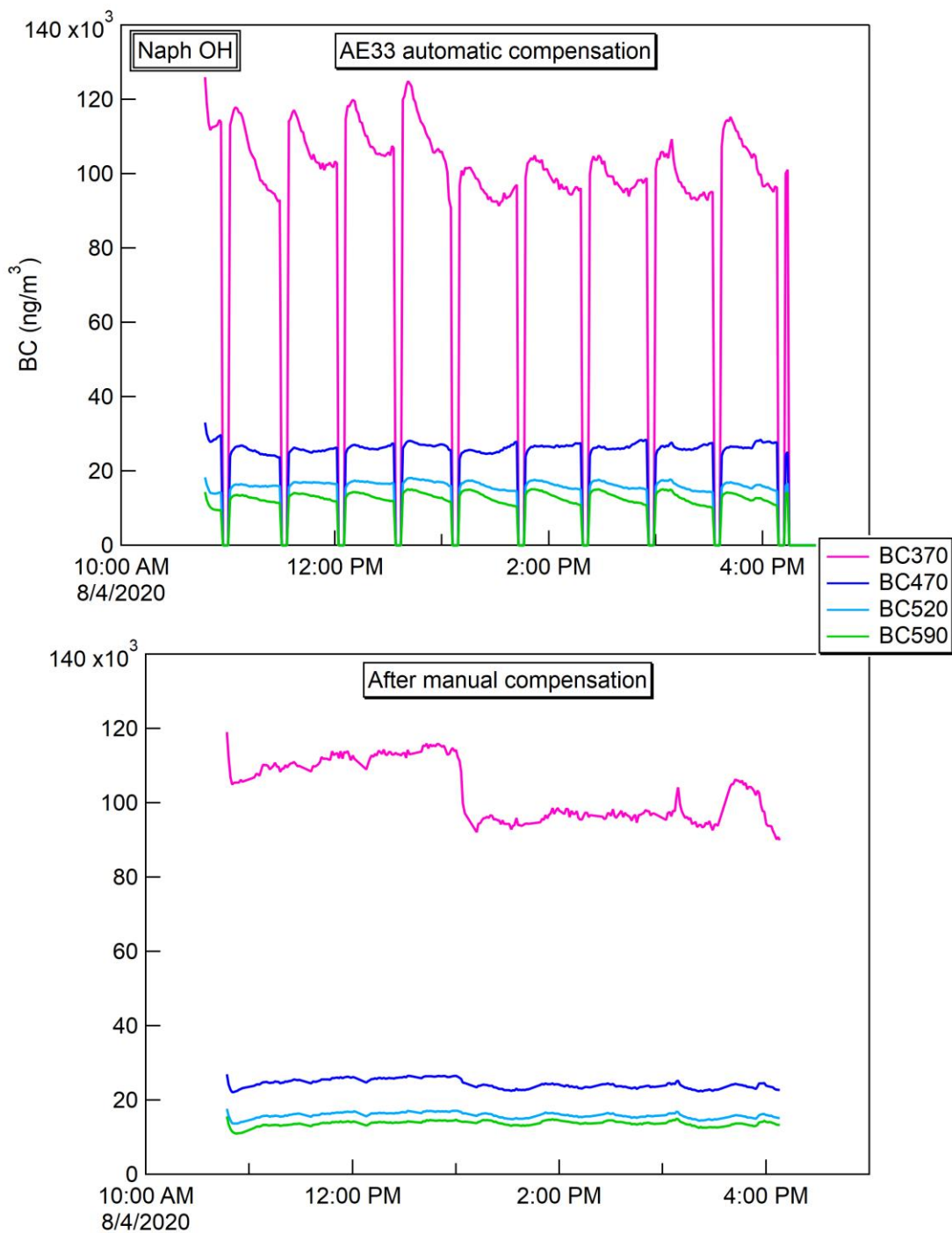
80

Figure S2. Modeled time series of OH, NO₃, and VOC as a function of the total residence time (τ) (KinSim model results). No results are shown for Furan and Flu with NO₃ radicals due to unstable SOA generation or no SOA formed.

Figure S3. Example of AE33 automatic compensation and manual compensation on the time evolution of BC concentrations measured at different wavelengths for Naph SOA produced with OH radical.

85
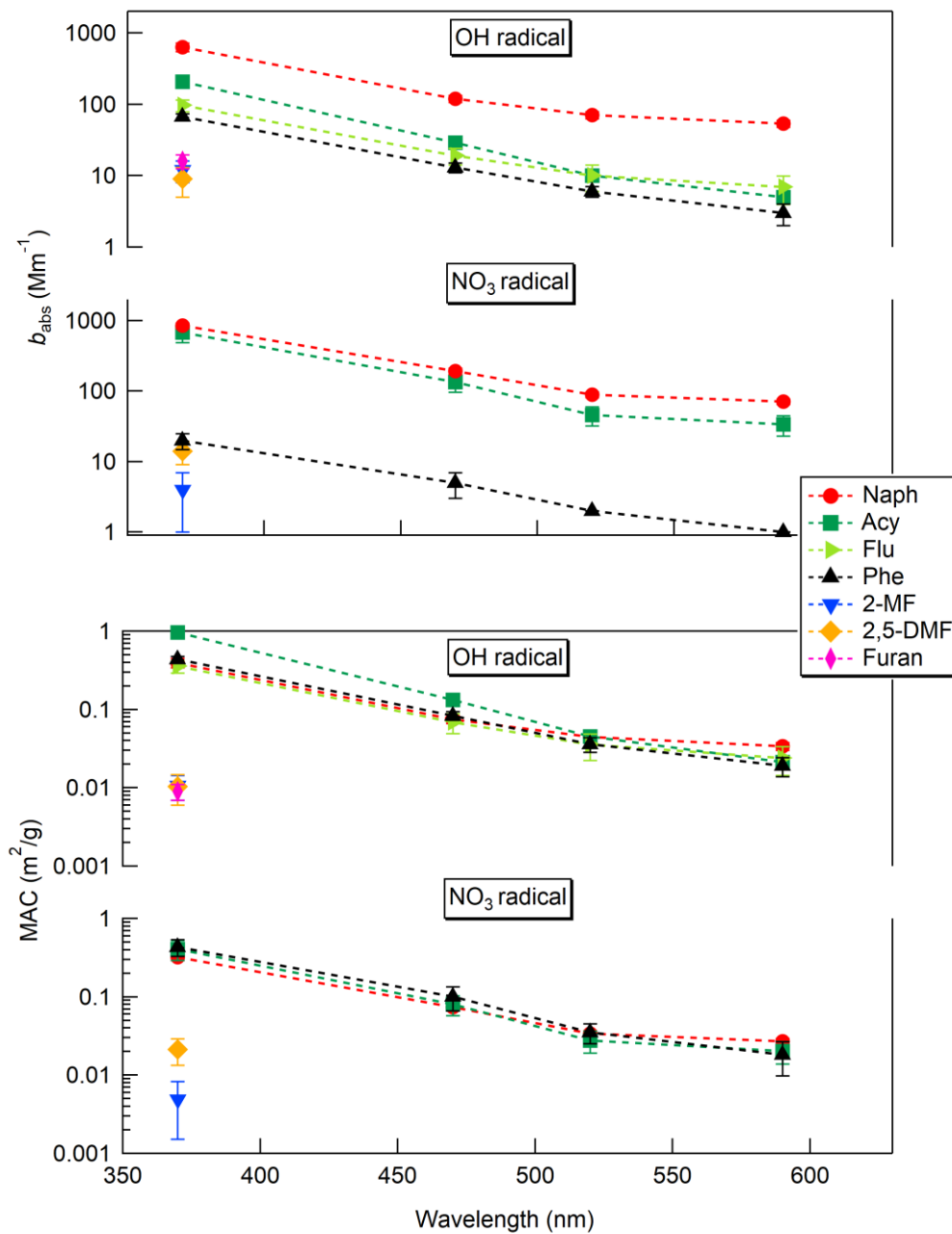
Figure S4. Comparison of wavelength-dependent absorption optical properties (b_{abs}, and MAC) of PAHs and furans SOA generated from the day- and nighttime oxidation processes (with OH and NO₃ radicals respectively). Results were plotted as a function of λ in the range of 370 to 590 nm. No results are shown for Furan and Flu with NO₃ radicals due to unstable SOA generation or no SOA formed.
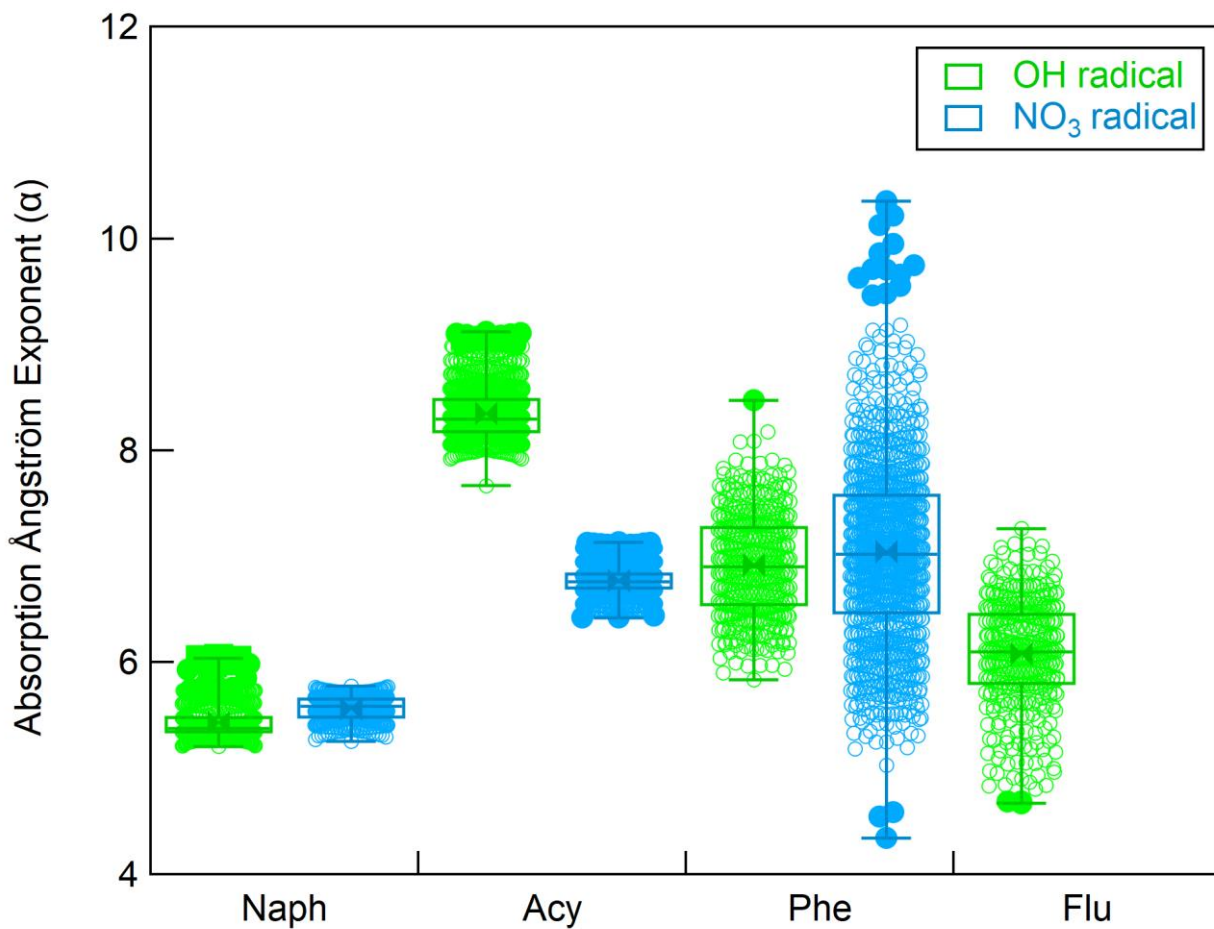
Figure S5. Variation of Absorption Ångström exponent (α) of the PAHs SOA generated from the day- and nighttime oxidation processes (with OH and NO₃ radicals respectively). No results are shown for Flu with NO₃ radicals because no SOA were formed.

REFERENCES

The MPI-Mainz UV/VIS Spectral Atlas of Gaseous Molecules of Atmospheric Interest: https://essd.copernicus.org/articles/5/365/2013/.

Database for the Kinetics of the Gas-Phase Atmospheric Reactions of Organic Compounds: https://data.eurochamp.org/data-access/kin/#/data.

Theoretical spectral database of PAHs: https://www.dsf.unica.it/~gmalloci/pahs/index.html.

Atkinson, R. and Aschmann, S. M.: Kinetics of the reactions of acenaphthene and acenaphthylene and structurally-related aromatic compounds with OH and NO_3 radicals, N_2O_5 and O_3 at 296 ± 2 K: KINETICS OF GAS-PHASE REACTIONS, Int. J. Chem. Kinet., 20, 513–539, https://doi.org/10.1002/kin.550200703, 1988.

Christianson, M. G., Doner, A. C., Koritzke, A. L., Frandsen, K., and Rotavera, B.: Vacuum-ultraviolet absorption cross-sections of functionalized cyclic hydrocarbons: Five-membered rings, Journal of Quantitative Spectroscopy and Radiative Transfer, 258, 107274, https://doi.org/10.1016/j.jqsrt.2020.107274, 2021.

Ding, Z., Yi, Y., Wang, W., and Zhang, Q.: Understanding the role of Cl and NO3 radicals in initiating atmospheric oxidation of fluorene: A mechanistic and kinetic study, Science of The Total Environment, 716, 136905, https://doi.org/10.1016/j.scitotenv.2020.136905, 2020.

Drinovec, L., Močnik, G., Zotter, P., Prévôt, A. S. H., Ruckstuhl, C., Coz, E., Rupakheti, M., Sciare, J., Müller, T., Wiedensohler, A., and Hansen, A. D. A.: The "dual-spot" Aethalometer: an improved measurement of aerosol black carbon with real-time loading compensation, Atmospheric Measurement Techniques, 8, 1965–1979, https://doi.org/10.5194/amt-8-1965-2015, 2015.

Giuliani, A., Delwiche, J., Hoffmann, S. V., Limão-Vieira, P., Mason, N. J., and Hubin-Franskin, M.-J.: 2-methyl furan: An experimental study of the excited electronic levels by electron energy loss spectroscopy, vacuum ultraviolet photoabsorption, and photoelectron spectroscopy, J. Chem. Phys., 119, 3670–3680, https://doi.org/10.1063/1.1590960, 2003.

Grosch, H., Sárossy, Z., Egsgaard, H., and Fateev, A.: UV absorption cross-sections of phenol and naphthalene at temperatures up to 500°C, Journal of Quantitative Spectroscopy and Radiative Transfer, 156, 17–23, https://doi.org/10.1016/j.jqsrt.2015.01.021, 2015.

He, Q., Li, C., Siemens, K., Morales, A. C., Hettiyadura, A. P. S., Laskin, A., and Rudich, Y.: Optical Properties of Secondary Organic Aerosol Produced by Photooxidation of Naphthalene under NOx Condition, Environ. Sci. Technol., 56, 4816–4827, https://doi.org/10.1021/acs.est.1c07328, 2022.

Jiang, J., Carter, W. P. L., Cocker, D. R. I., and Barsanti, K. C.: Development and Evaluation of a Detailed Mechanism for Gas-Phase Atmospheric Reactions of Furans, ACS Earth Space Chem., 4, 1254–1268, https://doi.org/10.1021/acsearthspacechem.0c00058, 2020.

Keyte, I. J., Harrison, R. M., and Lammel, G.: Chemical reactivity and long-range transport potential of polycyclic aromatic hydrocarbons – a review, Chem. Soc. Rev., 42, 9333, https://doi.org/10.1039/c3cs60147a, 2013.

Kind, I., Berndt, T., Böge, O., and Rolle, W.: Gas-phase rate constants for the reaction of NO3 radicals with furan and methyl-substituted furans, Chemical Physics Letters, 256, 679–683, https://doi.org/10.1016/0009-2614(96)00513-1, 1996.

Kitagawa, T.: Absorption spectra and photoionization of polycyclic aromatics in vacuum ultraviolet region, Journal of Molecular Spectroscopy, 26, 1–23, https://doi.org/10.1016/0022-2852(68)90139-2, 1968.

135 Klodt, A., Aiona, P., MacMillan, A., Lee, H. J. (Julie), Zhang, X., Helgestad, T., Novak, G., Lin, P., Laskin, J., Laskin, A., Bertram, T., Cappa, C., and Nizkorodov, S. A.: Effect of Relative Humidity, NOx, and Ammonia on Physical Properties of Naphthalene Secondary Organic Aerosol, Environ. Sci.: Atmos., https://doi.org/10.1039/D3EA00033H, 2023.

Kwok, E. S. C., Harger, W. P., Arey, Janet., and Atkinson, Roger.: Reactions of Gas-Phase Phenanthrene under Simulated Atmospheric Conditions, Environ. Sci. Technol., 28, 521–527, https://doi.org/10.1021/es00052a027, 1994.

140 Kwok, E. S. C., Atkinson, R., and Arey, J.: Kinetics of the gas-phase reactions of indan, indene, fluorene, and 9,10-dihydroanthracene with OH radicals, NO3 radicals, and O3, International Journal of Chemical Kinetics, 29, 299–309, https://doi.org/10.1002/(SICI)1097-4601(1997)29:4<299::AID-KIN9>3.0.CO;2-P, 1997.

Lambe, A. T., Cappa, C. D., Massoli, P., Onasch, T. B., Forestieri, S. D., Martin, A. T., Cummings, M. J., Croasdale, D. R., Brune, W. H., Worsnop, D. R., and Davidovits, P.: Relationship between Oxidation Level and Optical Properties of Secondary
145 Organic Aerosol, Environ. Sci. Technol., 47, 6349–6357, https://doi.org/10.1021/es401043j, 2013.

Lee, H. J. (Julie), Aiona, P. K., Laskin, A., Laskin, J., and Nizkorodov, S. A.: Effect of Solar Radiation on the Optical Properties and Molecular Composition of Laboratory Proxies of Atmospheric Brown Carbon, Environ. Sci. Technol., 48, 10217–10226, https://doi.org/10.1021/es502515r, 2014.

Li, M., Liu, Y., and Wang, L.: Gas-phase ozonolysis of furans, methylfurans, and dimethylfurans in the atmosphere, Phys.
150 Chem. Chem. Phys., 20, 24735–24743, https://doi.org/10.1039/C8CP04947E, 2018.

Metcalf, A. R., Loza, C. L., Coggon, M. M., Craven, J. S., Jonsson, H. H., Flagan, R. C., and Seinfeld, J. H.: Secondary Organic Aerosol Coating Formation and Evaporation: Chamber Studies Using Black Carbon Seed Aerosol and the Single-Particle Soot Photometer, Aerosol Science and Technology, 47, 326–347, https://doi.org/10.1080/02786826.2012.750712, 2013.

Rowe, J. P., Lambe, A. T., and Brune, W. H.: Technical Note: Effect of varying the $\lambda = 185$ and 254 nm photon flux ratio on
155 radical generation in oxidation flow reactors, Atmospheric Chemistry and Physics, 20, 13417–13424, https://doi.org/10.5194/acp-20-13417-2020, 2020.

Siemens, K., Morales, A., He, Q., Li, C., Hettiyadura, A. P. S., Rudich, Y., and Laskin, A.: Molecular Analysis of Secondary Brown Carbon Produced from the Photooxidation of Naphthalene, Environ. Sci. Technol., 56, 3340–3353, https://doi.org/10.1021/acs.est.1c03135, 2022.

160 Updyke, K. M., Nguyen, T. B., and Nizkorodov, S. A.: Formation of brown carbon via reactions of ammonia with secondary organic aerosols from biogenic and anthropogenic precursors, Atmospheric Environment, 63, 22–31, https://doi.org/10.1016/j.atmosenv.2012.09.012, 2012.

Xie, M., Chen, X., Hays, M. D., Lewandowski, M., Offenberg, J., Kleindienst, T. E., and Holder, A. L.: Light Absorption of Secondary Organic Aerosol: Composition and Contribution of Nitroaromatic Compounds, Environ. Sci. Technol., 51, 11607–
165 11616, https://doi.org/10.1021/acs.est.7b03263, 2017.